Accelerated river avulsion frequency on lowland deltas due to sea-level rise

Austin J. Chadwick[a,1], Michael P. Lamb[a], and Vamsi Ganti[b,c]

[a]Division of Geological and Planetary Sciences, California Institute of Technology, Pasadena, CA 91125; [b]Department of Geography, University of California, Santa Barbara, CA 93106; and [c]Department of Earth Science, University of California, Santa Barbara, CA 93106

Edited by Andrea Rinaldo, École Polytechnique Fédérale de Lausanne, Lausanne, Switzerland, and approved June 3, 2020 (received for review July 17, 2019)

Sea-level rise, subsidence, and reduced fluvial sediment supply are causing river deltas to drown worldwide, affecting ecosystems and billions of people. Abrupt changes in river course, called avulsions, naturally nourish sinking land with sediment; however, they also create catastrophic flood hazards. Existing observations and models conflict on whether the occurrence of avulsions will change due to relative sea-level rise, hampering the ability to forecast delta response to global climate change. Here, we combined theory, numerical modeling, and field observations to develop a mechanistic framework to predict avulsion frequency on deltas with multiple self-formed lobes that scale with backwater hydrodynamics. Results show that avulsion frequency is controlled by the competition between relative sea-level rise and sediment supply that drives lobe progradation. We find that most large deltas are experiencing sufficiently low progradation rates such that relative sea-level rise enhances aggradation rates—accelerating avulsion frequency and associated hazards compared to preindustrial conditions. Some deltas may face even greater risk; if relative sea-level rise significantly outpaces sediment supply, then avulsion frequency is maximized, delta plains drown, and avulsion locations shift inland, posing new hazards to upstream communities. Results indicate that managed deltas can support more frequent engineered avulsions to recover sinking land; however, there is a threshold beyond which coastal land will be lost, and mitigation efforts should shift upstream.

sea-level rise | river deltas | river avulsion

Coastal cities and wetlands are drowning due to global sea-level rise, accelerated subsidence from fluid extraction, and reduced fluvial sediment supply (1–3), with significant implications for the global economy, carbon cycle, and diverse ecosystems (4–6). Most estimates of coastal inundation for the coming century do not consider the land-building potential of riverine sedimentation (7–9). Rivers naturally distribute sediment across deltaic plains through avulsions—catastrophic shifts in the river course—which occur every 10 to 1,000 years on different deltas (Fig. 1 *A* and *B*) (10, 11). However, it is unknown what sets avulsion timescales and how avulsion occurrence will change with increasing rates of relative sea-level rise caused by climate and land-use changes (12, 13). River avulsions counter land loss by nourishing wetlands with sediment (14) but also have caused some of the deadliest floods in human history (10, 15, 16). On densely populated fluvial systems, dammed reservoirs trap sediment and engineered levees prevent avulsions, with the unintended consequence of heightened land loss (8, 9). Engineered river diversions are now important parts of future billion-dollar coastal restoration plans (17). Despite their global importance, we lack a predictive framework for avulsion reoccurrence on deltas, which is imperative to mitigate catastrophic flood hazards and design effective diversions on engineered deltas (8, 9).

Existing observations and models produce conflicting results as to whether avulsion frequency will increase or decrease with relative sea-level rise. For example, avulsion frequency on the Rhine–Meuse delta increased during late Holocene sea-level rise (19), consistent with observations in fan-delta experiments (20). In contrast, avulsion frequency decreased on the Mitchell River delta during Holocene sea-level rise (21). Similarly, numerical model predictions differ on whether avulsions on the Mississippi and Trinity Rivers were more or less frequent during the Holocene period (22, 23) despite their geographic proximity (24). Sequence stratigraphic models (25) and physical experiments (26) predict sea-level fall causes valley incision preventing avulsion, whereas the Goose River delta (27) represents an example where avulsions persisted during sea-level fall.

Previous work documented that the characteristic avulsion frequency, f_A, scales with the rate that the riverbed aggrades to a height comparable to its channel depth,

$$f_A = \frac{v_a}{H}, \quad [1]$$

where v_a is the in-channel aggradation rate, $H = H^*H_c$ is the aggradation thickness necessary for avulsion, and H_c is the bankfull channel depth (28, 29). The avulsion threshold, H^*, is a dimensionless number between 0.2 and 1.4 on lowland deltas (30). Aggradation rates, in contrast, span orders of magnitude (v_a = 0.5 to 100 mm/y; ref. 29). Thus, river avulsions may occur as frequently as every decade (e.g., the Huanghe; Fig. 1*A* and ref. 31) or as rarely as each millennium (e.g., the Mississippi; Fig. 1*B* and ref. 32), and Eq. **1** is only useful insofar as aggradation rate can be predicted.

Analytical models are often used to approximate v_a through spatial averaging of sediment mass balance. A common approach

Significance

River deltas host large cities and ecosystems and are sinking under global sea-level rise and land subsidence from groundwater and hydrocarbon extraction. Coastal rivers naturally build land by distributing sediment through abrupt shifts in river course, known as avulsions, which also have caused some of deadliest flood disasters in human history. We show that modern rates of relative sea-level rise should cause avulsions to occur more frequently on deltas, and in extreme cases avulsion locations will shift farther inland. Our results provide a quantitative framework to predict delta response to future sea-level rise, which is valuable for planning engineered diversions to nourish deltas and prevent catastrophic hazards.

Author contributions: A.J.C., M.P.L., and V.G. designed research; A.J.C. and M.P.L. performed research; A.J.C. and M.P.L. analyzed data; and A.J.C., M.P.L., and V.G. wrote the paper.

The authors declare no competing interest.

This article is a PNAS Direct Submission.

Data deposition: The data and model code underlying this study are publicly available in the SEAD Repository (http://doi.org/10.26009/s0FSLKFK) and GitHub (https://github.com/achadwick2323/Accelerated-river-avulsion-frequency-on-lowland-deltas-due-to-sea-level-rise), respectively.

[1]To whom correspondence may be addressed. Email: achadwick@caltech.edu.

This article contains supporting information online at https://www.pnas.org/lookup/suppl/doi:10.1073/pnas.1912351117/-/DCSupplemental.

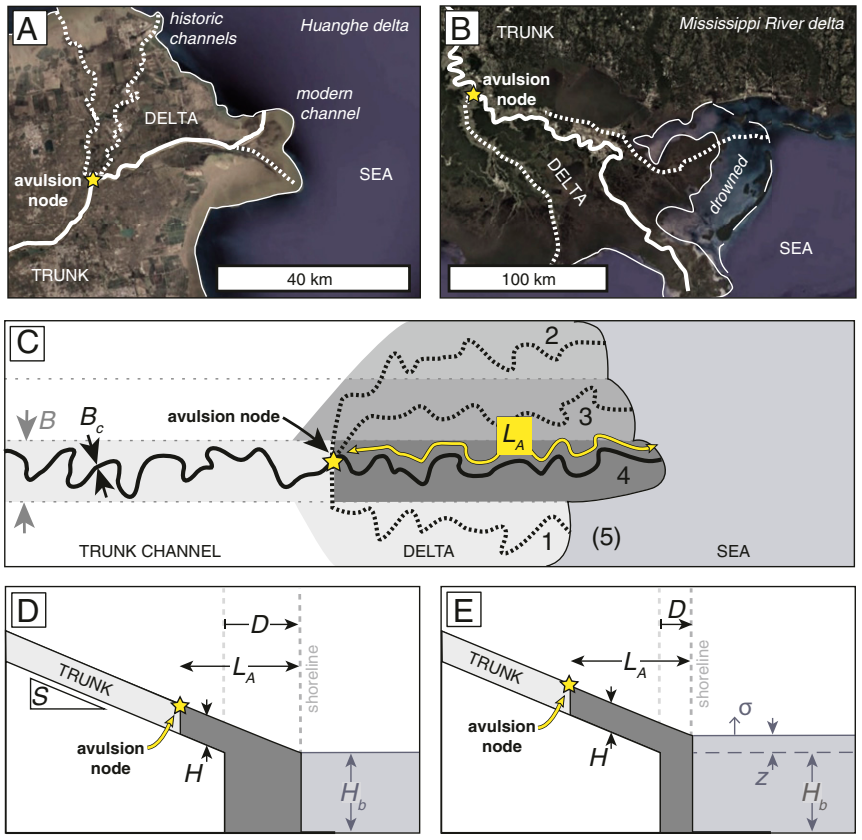

Fig. 1. Natural and modeled deltas. (*A*) Huanghe delta, China and (*B*) Mississippi River delta, United States, showing modern (solid line) and abandoned (dotted line) channel pathways and avulsion node (yellow star) (Google Earth). The thin dashed line in *B* indicates approximate shoreline before human management (18). (*C*) Model conceptualization, showing channels of width B_c that occupy lobes of width B (shaded regions) and length L_A (yellow line). Shaded regions are deposits created during avulsion cycles 1 through 4. Once the channel avulses from the active lobe 4 to the space 5, all lateral accommodation is filled, and the avulsion node moves downstream in tandem with progradation. (*D*) Model conceptualization in cross-section for constant relative sea level and (*E*) relative sea-level rise rate of σ, showing lobe length L_A, lobe-progradation distance D, topset slope S, basin depth H_b, relative sea-level rise magnitude z, and aggradation height H in a single avulsion cycle on the active lobe (gray shaded region).

to estimate v_a is a radially averaged model, in which the delta apex is geographically fixed and relative sea-level rise causes the delta radius to shrink until sediment supply is sufficient to keep delta-top aggradation at pace with sea level (8, 11, 33–38). At steady state, the delta land area is given by $A_\Delta = \frac{1}{(1-\lambda_p)}\frac{Q_s}{\sigma}$, where Q_s is the volumetric sediment supply, σ is the relative sea-level rise rate, and λ_p is the deposit porosity (8, 11). Aggradation rate is given by

$$v_a = \frac{1}{(1-\lambda_p)}\frac{Q_s}{A_\Delta} = \sigma. \qquad [2]$$

For the radially averaged model, aggradation is enhanced during marine transgression because, with a fixed delta apex and sediment supply, the delta land area is reduced (33, 39). Eq. **2** shows agreement with steep experimental deltas where the delta apex was geographically fixed by a canyon-fan transition or flume inlet (20, 37). In contrast to steep fan deltas, lowland deltas have an apex that is not fixed but instead is found at a characteristic distance upstream of the shoreline where avulsions preferentially occur due to backwater hydrodynamics (22, 31, 40, 41). It is unknown if lowland deltas will change their area to equilibrate with sediment supply and sea-level rise as indicated by Eq. **2**, or if delta response will differ because backwater hydrodynamics set a constant lobe length (41, 42).

A second analytical approach, termed the channel-averaged model, is to constrain aggradation rate using sediment mass balance for a channel. For example, Reitz et al. (43) found avulsions occurred in a fan-delta experiment at the rate the sediment supply could fill the channel: $\frac{1}{(1-\lambda_p)}Q_sT_A = HB_cL_A$, where T_A is the time between avulsions, B_c is channel width, and L_A is delta lobe length—the distance upstream from the shoreline where avulsions occur (Fig. 1*C*). Combined with Eq. **1** and $1/f_A \equiv T_A$, aggradation rate is given by

$$v_a = \frac{1}{(1-\lambda_p)}\frac{Q_s}{L_AB_c}. \qquad [3]$$

In Eq. **3**, B_c can be substituted by an effective delta lobe width, B, to approximate lateral distribution of sediment across a delta lobe, for example due to bifurcations (35, 44–48). While the channel-averaged model considers sedimentation within a discrete channel or lobe, it does not account for backwater hydrodynamics, multiple lobes, or sediment partitioning between lobe aggradation and progradation.

More complex two-dimensional (2D) morphodynamic models designed to study delta bifurcations and channelization (14, 27, 49–53) have yet to be run systematically to explore backwater-scaled avulsions. While simpler one-dimensional morphodynamic models that include backwater hydrodynamics exist, these models are tuned to specific case studies (22, 23) and yielded opposite trends for avulsion frequency response to relative sea-level rise. A 2D reduced-complexity model found that avulsion

frequency was insensitive to sea-level rise for small rise rates due to progradation (54). However, this model did not include backwater hydrodynamics or a model spin-up phase. A spin-up phase was shown to eliminate bias in predicted avulsion locations associated with the assumed initial topography, by reworking the initial topography for at least one avulsion cycle per delta lobe (55).

Recent models for backwater-scaled avulsions have included quasi-2D nonuniform flow, lobe aggradation and progradation, multiple cycles of lobe growth and abandonment, and a spin-up phase (55, 56). These models provided new insight into the controls on avulsion location on deltas (55) and were validated against field observations from the Huanghe delta (56); however, they have yet to be used to explore how relative sea-level rise affects avulsion frequency. Here we built on the model of Chadwick et al. (55) to develop a generic framework to predict the response of avulsion frequency on deltas to different rates of relative sea-level rise and fall. We also derived an analytical approximation to the model that can be directly compared to the commonly used radially averaged and channel-averaged approximations.

Backwater-Scaled-Avulsion Modeling and Field Data. The numerical morphodynamic model for avulsions consisted of a delta composed of multiple lobes that were assumed to form a branching pattern (Fig. 1*C*) (30, 55) (*SI Appendix*, section A). We represented each lobe by a separate long profile and a shared trunk channel, and only one lobe was active at a given time. The evolution of the active lobe was governed by quasi-2D nonuniform hydrodynamics (22), sediment transport (57), and sediment mass balance of the lobe topset and foreset (58). Avulsions occurred when and where the active lobe first aggraded to a specified height H relative to the lowest neighboring lobe (Eq. **1**) (22, 28, 41, 54). Subsequently, the active channel was rerouted downstream and the lowest-elevation abandoned lobe became the new active lobe (*SI Appendix*, section A). Inactive lobes were unchanged, except for inundation due to relative sea-level rise, approximating a river-dominated delta with negligible reworking from waves or currents (54, 56). Every model run began with a spin-up phase in which the river occupied each lobe at least once, thereby eliminating the bias of the imposed initial conditions (55) (*SI Appendix*, section B).

Dimensional analysis revealed that model behavior depended primarily on the ratio of rates of relative sea-level rise and sediment supply to the delta. We termed this dimensionless parameter the normalized relative sea-level rise rate, $\sigma^* = \frac{\sigma}{Q_s/nL_bB(1-\lambda_p)}$, where $n = (N+1)/2$, N is the number of delta lobes, $L_b = H_c/S$ is the backwater length scale, and S is channel bed slope (*SI Appendix*, sections A and C). Delta lobe progradation occurs for $\sigma^* < 1$, and when $\sigma^* > 1$ the shoreline retreats and the delta lobe drowns. Delta response also depends on the offshore basin depth (H_b) relative to the channel depth (Fig. 1*D*), the lobe width (B) relative to the channel width, the avulsion threshold ($H^* = H/H_c$), and six additional dimensionless parameters that describe river flow hydraulics and sediment transport (*SI Appendix*, section B). For each modeled delta, we computed the average time between avulsions (T_A) over 13 avulsion cycles and calculated $f_A \equiv 1/T_A$ under different scenarios of normalized relative sea-level rise rate (σ^*), with all other parameters held constant at values representative of typical lowland deltas (*SI Appendix*, section B and Tables S1 and S2).

We also derived an independent analytical model for avulsion frequency by setting lobes to a fixed length scaled by L_b (22, 40) and averaging sediment mass balance over an avulsion timescale for a river channel of constant slope (*SI Appendix*, section D). These assumptions circumvented the need to solve the nonlinear equations for water and sediment transport. The result is

$$f_A = \begin{cases} \dfrac{1}{(1-\lambda_p)} \dfrac{Q_s}{(L_A - D)BH + DB\left(H_b + z + DS/2\right)} & \text{if } D \geq 0 \\ \dfrac{1}{(1-\lambda_p)} \dfrac{Q_s}{L_A BH} & \text{if } D < 0 \end{cases} \quad [4]$$

where $D = (H - z)/S$ is the lobe-progradation distance and $z = n\sigma f_A^{-1}$ is the magnitude of relative sea-level rise during an interavulsion period (Fig. 1 *D* and *E* and *SI Appendix*, section C). The lobe length, L_A, typically varies between $0.5L_b$ and $2L_b$ for large, coastal rivers (30, 55), and in Eq. **4** it is a specified constant, unlike in the numerical model where L_A is a model outcome that emerges due to backwater hydrodynamics (55). For $D \geq 0$, the first and second terms in the denominator account for sediment partitioned to the lobe topset and foreset, respectively. For $D < 0$, all sediment is sequestered in the topset. We used the analytical solution as a comparison to the numerical model and to explore the effect of relative sea-level rise on avulsion frequency with covarying basin depth, avulsion threshold, lobe length, and lobe width.

We compared the numerical and analytical models to a compilation of data from 15 natural deltas spanning a wide range of known avulsion frequencies $\left(f_A = 0.5 \text{ to } 140 \text{ ky}^{-1}\right)$ and lobe lengths ($L_A = 30$ to 490 km; *SI Appendix*, Tables S1 and S2; refs. 21, 23, 27, and 29). Due to infrequent historical avulsions, documented avulsions pertain to the Holocene period, with the exception of the Huanghe where historic natural avulsions were documented between 1889 and 1930 prior to major engineering (Fig. 1*A*) (31). Consistent with our model assumptions, these deltas feature a single major channel and lobe lengths that scale with the backwater length (22, 45). For each delta, we computed the average relative sea-level rise rate during the period of avulsions as the sum of eustatic sea-level rise rate (σ_{eu}) and coastal subsidence rate (σ_{subs}), that is, $\sigma = \sigma_{eu} + \sigma_{subs}$ (4, 59–63). We used available data to constrain reasonable values for other model inputs ($H^* = 0.5, L_A = L_b, H_b = 2H_c$) and to test model results against avulsion frequencies for six deltas where all model inputs could be constrained (*SI Appendix*, Table S2). We also computed modern expectations for avulsion frequency using relative sea-level rise rates for each delta measured by tide gauges over the 20th century (64). All calculations used historical measurements to estimate river sediment loads prior to damming (65). To facilitate comparison to natural deltas, the model and data were normalized through dimensional analysis (*SI Appendix*, sections A and D and Table S2). Results were cast in terms of normalized avulsion frequency, $f_A^* = \frac{f_A}{Q_s/H_cB_cL_b(1-\lambda_p)}$, which approaches unity when the sediment supply is entirely sequestered in the delta lobe topset, rather than the foreset.

Results

Results from backwater-scaled-avulsion modeling show that avulsion frequency responds nonlinearly to relative sea-level rise rate, falling within three regimes depending on the competition between relative sea-level rise and sediment supply as described by σ^* (Fig. 2). In the regime $10^{-4} < \sigma^* \lesssim 10^{-1}$, termed progradation-dominated, sediment supply outpaces the accommodation space created on the delta top due to relative sea-level rise, causing lobe progradation (Fig. 1*E* and *SI Appendix*, Fig. S1). Lobe progradation causes channel aggradation because the channel adjusts to maintain a transport slope as the river mouth and avulsion node advance seaward (31). Because avulsion frequency scales with aggradation rate (Eq. **1**), f_A is insensitive to relative

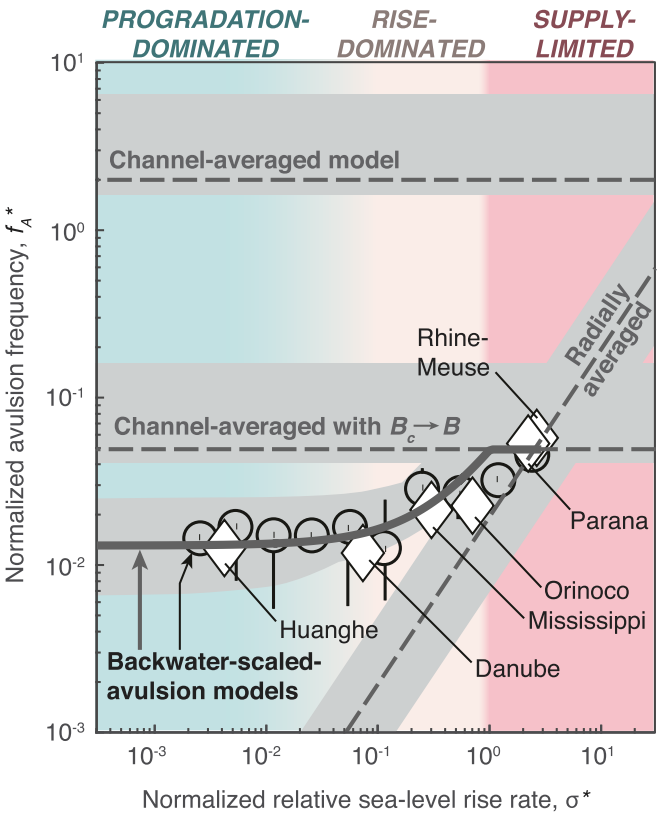

Fig. 2. Normalized avulsion frequency, f_A^*, versus normalized relative-sea level rise rate, σ^*. Black circles and error bars show the median, minimum, and maximum from 13 avulsions that occurred for each backwater-scaled numerical model run. The gray solid line is the backwater-scaled analytical model (Eq. **4**), and dashed lines are radially averaged model (Eq. **2**), channel-averaged model (Eq. **3**), and channel-averaged model incorporating a lobe width (Eq. **3** with $B_c \rightarrow B$) with other variables set to constant values typical of large lowland deltas ($H^* = 0.5, L_A = L_b, H_b = 2H_c, N = 4,$ and $B = 40B_c$; *SI Appendix*, Table S2). White diamonds are data for Holocene avulsions on natural deltas and preindustrial historical avulsions on the Huanghe, where all parameters are constrained, and gray shaded regions are envelopes of analytical model solutions for input parameters corresponding to each natural delta (*SI Appendix*, section B and Table S2).

sea-level rise in this regime (Fig. 2), similar to previous reduced-complexity model results (54).

Results indicate that channel aggradation increases with relative sea-level rise when the rates of relative sea level rise and sediment supply are similar $\left(10^{-1} \lesssim \sigma^* < 10^{0}\right)$ (Fig. 2 and *SI Appendix*, Fig. S1). In this regime, termed rise-dominated, relative sea-level rise enhances channel aggradation because more sediment is partitioned into the lobe topset relative to the foreset, in a process similar to the radially averaged model (8, 37, 38, 58), but here manifesting at the scale of delta lobes. Consequently, avulsion frequency accelerates as relative sea-level rise rate increases (Fig. 2).

For $\sigma^* > 10^{0}$, relative sea-level rise outpaces the rate at which the sediment supply can aggrade the reach downstream of the avulsion node, causing coastal land to drown and the avulsion node to shift upstream. In this regime, termed supply-limited, aggradation rate and rise rate are decoupled. Instead, aggradation rate is limited by the sediment supply per unit lobe area (i.e., the product of lobe length L_A and width B), and avulsion frequency reaches a maximum value that is insensitive to rise rate (Fig. 2).

Independently varying parameters in the analytical model revealed that relative sea-level rise universally increases avulsion frequency in the rise-dominated regime ($0.1 \lesssim \sigma^* < 1$) by creating accommodation space at a rate commensurate with the sediment supply (Fig. 3). Smaller basin depths also increase avulsion frequency (Fig. 3*A*), but only for low rise rates. Small basin depths facilitate rapid progradation when $\sigma^* \lesssim 0.1$, driving high aggradation rates on the topset to maintain a transport slope. Results show that avulsion frequency increases with decreasing avulsion threshold and lobe length (Fig. 3 *B* and *C*) because less sediment is needed on the delta top to cause an avulsion. Avulsion frequency decreases as lobe width increases (Fig. 3*D*), consistent with the recent finding that wider distributary networks are more resilient to environmental change (47). When rapid relative sea-level rise causes marine transgression ($D < 0$), the sediment supplied to the delta lobe is entirely sequestered on the lobe top, and f_A is maximized to a value controlled by lobe length (L_A), width (B), and aggradation thickness necessary for an avulsion (H) (Eq. **4**). For cases with shallow basins and $L_A/L_b >> 1$, such as steep fan deltas (31), avulsion frequency is insensitive to σ^* because the large topset area causes a transition from progradation-dominated to supply-limited conditions at relatively low rise rates (Fig. 3*C*). For $\sigma^* \gtrsim 2.5$, the avulsion node drowns before in-channel sedimentation can reach the avulsion threshold.

Model results also indicate that avulsions can occur during relative sea-level fall, so long as the channel is aggradational (Fig. 3*E*) (27, 66). Basin depth is the fundamental control on avulsion frequency during sea-level fall because topset aggradation is driven primarily by lobe progradation, similar to the case of slow relative sea-level rise.

Our analytical model incorporates the crucial component of a backwater-scaled avulsion node that fixes the lobe length, consistent with the numerical model results and natural lowland deltas (Fig. 2). The backwater-scaled avulsion node moves seaward or landward in tandem with shoreline progradation or retreat, consistent with field observations (31, 56). Consequently, lobe length remains constant, and the competition between shoreline progradation, relative sea-level rise, and sediment supply controls avulsion frequency. The radially averaged model, in contrast, fixes the avulsion location such that shoreline progradation and retreat cause adjustment of delta top area, which scales inversely with the aggradation rate and avulsion frequency (Eq. **2** and Fig. 2 and *SI Appendix*, Fig. S2). The radially averaged model and our backwater-scaled-avulsion models produce qualitatively similar trends only in the rise-dominated regime $\left(10^{-1} \lesssim \sigma^* < 10^{0}\right)$; our model predicts more frequent avulsions in this regime due to additional topset aggradation from progradation that is not included in the radially averaged model. The channel-averaged model predicts $f_A^* = 2$ regardless of rise rate because all sediment is sequestered in the channel (Fig. 2 and *SI Appendix*, Fig. S2). Replacing channel width, B_c, in Eq. **3** with lobe width, B, yields predictions similar to our backwater-scaled-avulsion model, but only in the supply-limited regime ($\sigma^* \geq 1$). For $\sigma^* < 1$, our model predicts fewer avulsions because it partitions sediment to the delta foreset, which diminishes channel aggradation rates.

Data for avulsions during the Holocene period for the Danube, Mississippi, Rhine–Meuse, Orinoco, and Paraná deltas and the preindustrial historical avulsions on the Huanghe (*SI Appendix*, Tables S1 and S2) fall within the prediction envelope of the analytical backwater-scaled-avulsion model (Fig. 2). The high sediment load of the Huanghe yielded $\sigma^* \cong 0.004$, placing it in the progradation-dominated regime, where avulsion frequency is insensitive to relative sea-level rise. Avulsions on the Danube, Mississippi, and Orinoco are predicted to have been in the rise-dominated regime, in which avulsion frequency increases with relative sea-level rise rate ($\sigma^* \cong 0.1$, 0.3, and 0.77, respectively). The Paraná and Rhine–Meuse were in the supply-limited regime ($\sigma^* \cong 2.3$ and 2.6, respectively), where avulsion frequency is

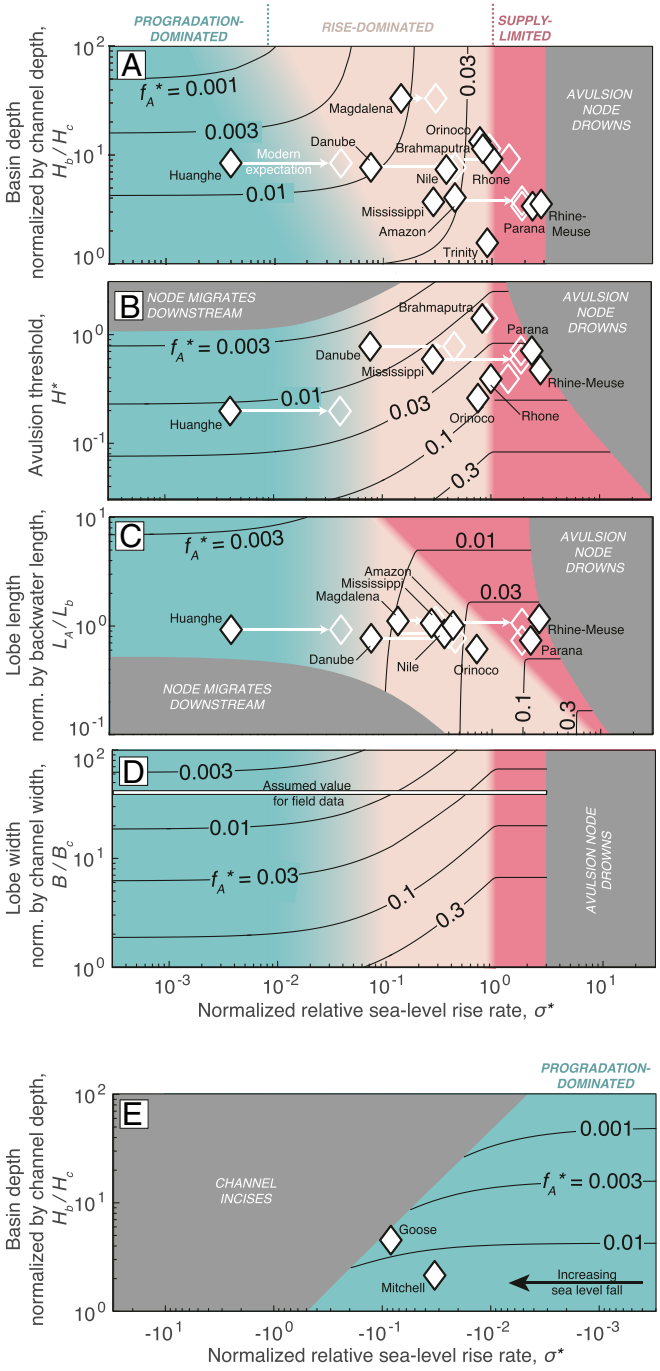

Fig. 3. Analytical model results for backwater-scaled avulsions. Contours of normalized avulsion frequency, f_A^*, as a function of normalized relative sea-level rise rate σ^* and (*A*) basin depth, (*B*) avulsion threshold, (*C*) lobe length, and (*D*) lobe width, with other variables set to constant values typical of large lowland deltas ($H^* = 0.5$, $L_A = L_b$, $H_b = 2H_c$, $N = 4$, $B = 40B_c$; *SI Appendix*, Table S2). (*E*) Solutions for falling sea level and varying basin depth. Gray zones indicate where the analytical model is not applicable due to shifting avulsion location or channel incision (*SI Appendix*, section D). White diamonds are data for preindustrial historical avulsions on the Huanghe and Holocene avulsions for the other deltas (filled markers; *SI Appendix*, Tables S1 and S2), and modern expectations based on rise rates documented over the 20th century (unfilled markers; *SI Appendix*, Table S3).

sensitive to sediment supply and delta size, and not to relative sea-level rise rate. While some model input parameters were unavailable for the other nine deltas in our compilation (*SI Appendix*, Table S2), they still can be placed within the model parameter space (Fig. 3). Model comparison suggests that the Nile, Magdalena, Amazon, Rhone, Brahmaputra, and Trinity deltas likely resided in the rise-dominated regime (Fig. 3 *A*–*D*), whereas the Goose and Mitchell deltas were in the progradation-dominated regime, such that avulsions occurred despite sea-level fall (Fig. 3*E*), consistent with observations (21, 27). We expect that accelerated relative sea-level rise over the past century (*SI Appendix*, Table S3) is causing many of these deltas to transition into the rise-dominated or supply-limited regimes (Fig. 3), which will result in either more frequent avulsions or avulsions that occur farther upstream.

Discussion and Conclusions

Our analytical and numerical models for backwater-scaled avulsions show that avulsion frequency on lowland deltas depends on the dominant cause of channel aggradation. To first order, avulsion frequency scales with the sediment supply to the delta and the delta top area [i.e., $f_A \propto Q_s/H_cB_cL_b(1-\lambda_p)$ or $f_A^* =$ constant], similar to the channel-averaged avulsion model (Fig. 2). However, our results indicate significant deviation from this scaling relation depending on whether channel aggradation is driven by progradation, relative sea-level rise, or limited by sediment supply (Figs. 2 and 3); these processes in turn determine whether or not avulsion frequency is sensitive to changes in relative sea-level rise rate. Our analytical model, despite its simplicity, accurately predicts avulsion frequencies observed in the physics-based numerical model (Fig. 2). Minor differences in mass balance arose because we assumed $L_A = L_b$ in the analytical model, whereas L_A in the numerical model emerged autogenically and varied between $0.5L_b$ and $2L_b$. Consistency between numerical and analytical model results (Fig. 2) suggests that the sediment partitioning between the delta topset and foreset exerts the primary control on avulsion frequency. Thus, beyond accounting for a backwater-scaled topset, modeling hydrodynamics and transient bed adjustment are not necessary to predict f_A to first order.

The parameter σ^* distinguishes between avulsion-frequency regimes because it compares the relative sea-level rise rate to the aggradation rate attained when sediment supplied to the delta lobe is entirely sequestered on the backwater-scaled topset (Fig. 4 *A*–*D*). Deltas with lobe lengths set by the backwater length ($L_A/L_b \sim 1$) feature a transition between the rise-dominated and supply-limited regimes at $\sigma^* = 1$, at which point lobe aggradation can only barely keep pace with sea-level rise. Similarly, $\sigma^* \approx 0.1$ marks a transition between the rise-dominated and progradation-dominated regimes. Our model indicates deltas may also transition between regimes as a result of increasing basin depth (H_b) and lobe length (L_A) associated with shoreline autoretreat (Fig. 3 *A* and *C*) (33, 39).

Our results have important implications for delta flood hazards and morphodynamics under changing σ^* and basin depth. Basin depth plays a significant role in the progradation-dominated regime ($\sigma^* \lesssim 0.1$) (Figs. 3*A* and 4) because less sediment is required for a given amount of progradation to occur in shallow basins (67–69). Thus, lowland deltas building into shallow epicontinental seas likely reside in the progradation-dominated regime and their avulsion frequency may be insensitive to relative sea-level rise. This model result can explain the puzzling observation of decreased avulsion frequency during Holocene sea-level rise on the Mitchell River delta (21), which builds into a shallow basin ($H_b = 15$ m) compared to the channel depth ($H_c = 7$ m). We reason that progradation rates may have decreased on the Mitchell delta as its basin deepened over the Holocene, causing less-frequent avulsions. In contrast, on deltas with deep offshore basins, such as shelf-edge deltas during sea-level lowstands (70), progradation is slow and so avulsion frequency should be more responsive to sea-level change.

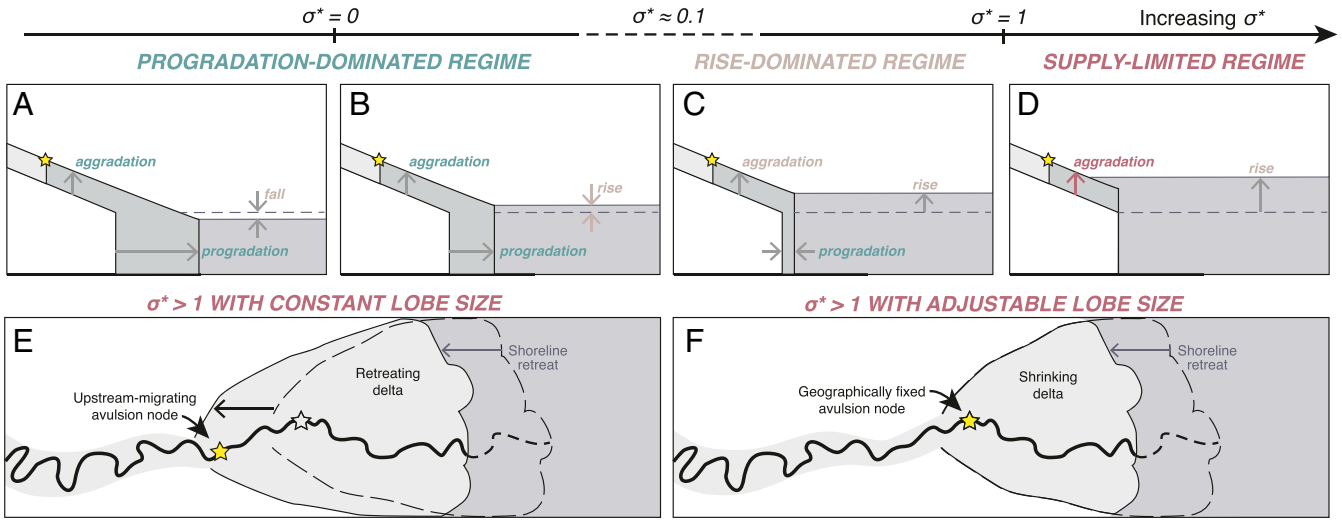

Fig. 4. Schematics of delta response to relative sea-level rise. Topographic profiles show locations of sediment deposition at the onset of avulsion under progradation-dominated (*A* and *B*), rise-dominated (*C*), and supply-limited (*D*) regimes, corresponding to increasing rates of normalized relative sea-level rise, σ^*. Planview schematics highlight different delta responses to rapid relative sea-level rise for (*E*) our model where deltas have a constant lobe length and (*F*) the radially averaged model where avulsion locations are fixed and delta lobes shrink.

Our model also shows that high progradation rates can drive channel aggradation and avulsion even during sea-level fall (Fig. 3*E*), which is typically thought to cause channel incision and prevent avulsion. This finding complicates sequence-stratigraphic interpretations of deltas building into shallow seas, such as the Cretaceous Interior Seaway (25), where unconformities interpreted as sequence boundaries reflecting sea-level fall could instead form intrinsically due to flood variability and avulsions (30, 71).

Our model indicates avulsion hazards should become more common and occur farther inland under modern rates of relative sea-level rise, as compared to over the Holocene. (Fig. 3 and *SI Appendix*, Table S3). Many deltas on continental shelves resided in the rise-dominated regime ($0.1 \lesssim \sigma^* < 1$) during the Holocene period, and so modern acceleration of rise rates is expected to cause more frequent avulsions (Fig. 3). More frequent avulsions will increase the potential for catastrophic flood hazards (15) but also present an opportunity to mimic natural processes on managed deltas by using engineered diversions to build land (8, 9, 17, 31). Results also point to distinct hazards associated with the supply-limited regime ($\sigma^* > 1$). Unlike radially averaged models with a geographically fixed avulsion node (Fig. 4*F*), the avulsion node in our model moves upstream when $\sigma^* > 1$ in order to keep pace with shoreline retreat and maintain a constant, backwater-scaled lobe length (Fig. 4*E*). Notably, under modern rise rates, the Mississippi and Rhone are predicted to transition to supply-limited conditions, similar to the Rhine–Meuse and Paraná (Fig. 3). As a result, we expect coastal land will drown, and shifting avulsion locations will introduce new flood hazards upstream of historic avulsion sites, such as at the Old River Control Structure on the Mississippi River (72). While the Huanghe has experienced a drastic increase in σ^* in the past century due to subsurface fluid extraction (64), our model indicates negligible change to avulsion frequency because aggradation is still predominantly set by progradation. Climate and land-use changes over the coming century are likely to further increase the rate of global sea-level rise, accelerate coastal subsidence, and reduce river sediment supply (4, 73), all of which can further amplify future avulsion hazards.

Overall our results indicate lowland deltas will not passively drown but instead will respond to relative sea-level rise through more frequent cycles of sedimentation and river avulsion (Fig. 4). While this response acts to mitigate land loss in coastal wetlands, it also heightens flood hazards. Engineered diversions that mimic rivers' natural tendency of more frequent avulsions during relative sea-level rise may offset land loss, but our results indicate there is a threshold beyond which sediment supply cannot keep pace with increasing rise rates, and avulsion hazards will shift upstream.

Materials and Methods

The numerical morphodynamic model solves the coupled equations for flow hydraulics, sediment transport, and topographic evolution (*SI Appendix*, sections A–C). The model is quasi-2D and assumes a specified number of lobes in a branching pattern. Only one lobe is active at a time, and the flow switches between lobes when aggradation reaches a critical value that triggers an avulsion, following ref. 55. The analytical model averages sediment mass balance over an avulsion cycle for a lobe that is assumed to build to a fixed length L_A set by backwater hydrodynamics (22, 40) with a constant riverbed slope (*SI Appendix*, section D). These assumptions allow for the prediction of avulsion frequency without solving nonlinear equations for water and sediment transport. Model parameters and avulsion frequencies for natural deltas were compiled from previous work (*SI Appendix*, Tables S1–S3).

ACKNOWLEDGMENTS. We thank Andrew Moodie, Gary Parker, Jeffrey Nittrouer, Hongbo Ma, and Brad Murray for useful discussions and three reviewers for constructive comments. We acknowledge NSF Grant EAR 1427262 and the Resnick Sustainability Institute at the California Institute of Technology for support.

1. R. J. Nicholls, A. Cazenave, Sea-level rise and its impact on coastal zones. *Science* **328**, 1517–1520 (2010).
2. W. K. Michener, E. R. Blood, K. L. Bildstein, M. M. Brinson, L. R. Gardner, Climate change, hurricanes and tropical storms, and rising sea level in coastal wetlands. *Ecol. Appl.* **7**, 770–801 (1997).
3. S. E. Darby *et al.*, Fluvial sediment supply to a mega-delta reduced by shifting tropical-cyclone activity. *Nature* **539**, 276–279 (2016).
4. J. P. M. Syvitski, Deltas at risk. *Sustain. Sci.* **3**, 23–32 (2008).
5. P. H. Gleick, Global freshwater resources: Soft-path solutions for the 21st century. *Science* **302**, 1524–1528 (2003).
6. C. S. Hopkinson, W.-J. Cai, X. Hu, Carbon sequestration in wetland dominated coastal systems—A global sink of rapidly diminishing magnitude. *Curr. Opin. Environ. Sustain.* **4**, 186–194 (2012).
7. Louisiana Coastal Wetlands Conservation and Restoration Task Force and the Wetlands Conservation and Restoration Authority, *Coast 2050: Toward a Sustainable Coastal Louisiana*, (Louisiana Dept. of Natural Resources, Baton Rouge, LA, 1998).

8. C. Paola *et al*., Natural processes in delta restoration: Application to the Mississippi Delta. *Annu. Rev. Mar. Sci.* **3**, 67–91 (2011).
9. W. Kim, D. Mohrig, R. R. Twilley, C. Paola, G. Parker, Is it feasible to build new land in the Mississippi River delta? *Eos (Wash. D.C.)* **90**, 373–374 (2009).
10. R. Slingerland, N. D. Smith, River avulsions and their deposits. *Annu. Rev. Earth Planet. Sci.* **32**, 257–285 (2004).
11. D. J. Jerolmack, Conceptual framework for assessing the response of delta channel networks to Holocene sea level rise. *Quat. Sci. Rev.* **28**, 1786–1800 (2009).
12. E. Rignot *et al*., Accelerated ice discharge from the Antarctic Peninsula following the collapse of Larsen B ice shelf. *Geophys. Res. Lett.* **31**, 2–5 (2004).
13. L. E. Erban, S. M. Gorelick, H. A. Zebker, Groundwater extraction, land subsidence, and sea-level rise in the Mekong Delta, Vietnam. *Environ. Res. Lett.* **9**, 84010 (2014).
14. D. A. Edmonds, D. C. Hoyal, B. A. Sheets, R. L. Slingerland, Predicting delta avulsions: Implications for coastal wetland restoration. *Geology* **37**, 759–762 (2009).
15. T. R. Kidder, H. Liu, Bridging theoretical gaps in geoarchaeology: Archaeology, geoarchaeology, and history in the Yellow River Valley, China. *Archaeol. Anthropol. Sci.* **9**, 1585–1602 (2017).
16. R. Sinha, The great avulsion of Kosi on 18 August 2008. *Curr. Sci.* **97**, 429–433 (2009).
17. Coastal Protection and Restoration Authority of Louisiana, "Integrated ecosystem restoration and hurricane protection: Louisiana's comprehensive master plan for a sustainable coast" (Coastal Protection and Restoration Authority of Louisiana, Baton Rouge, LA, 2007).
18. S. M. Gagliano, K. J. Meyer-Arendt, K. M. Wicker, Land loss in the Mississippi River deltaic plain. *GCAGS Trans.* **31**, 295–300 (1981).
19. T. E. Törnqvist, Middle and late Holocene avulsion history of the river Rhine (Rhine-Meuse delta, Netherlands). *Geology* **22**, 711–714 (1994).
20. J. Martin, B. Sheets, C. Paola, D. Hoyal, Influence of steady base-level rise on channel mobility, shoreline migration, and scaling properties of a cohesive experimental delta. *J. Geophys. Res.* **114**, F03017 (2009).
21. T. I. Lane, R. A. Nanson, B. K. Vakarelov, R. B. Ainsworth, S. E. Dashtgard, Evolution and architectural styles of a forced-regressive Holocene delta and megafan, Mitchell River, Gulf of Carpentaria, Australia. *Geol. Soc. Lond. Spec. Publ.* **444**, 305–334 (2017).
22. P. Chatanantavet, M. P. Lamb, J. A. Nittrouer, Backwater controls of avulsion location on deltas. *Geophys. Res. Lett.* **39**, L01402 (2012).
23. K. E. Moran, J. A. Nittrouer, M. M. Perillo, J. Lorenzo-Trueba, J. B. Anderson, Morphodynamic modeling of fluvial channel fill and avulsion time scales during early Holocene transgression, as substantiated by the incised valley stratigraphy of the Trinity River, Texas. *J. Geophys. Res. Earth Surf.* **122**, 215–234 (2017).
24. J. B. Anderson, D. J. Wallace, A. R. Simms, A. B. Rodriguez, K. T. Milliken, Variable response of coastal environments of the northwestern Gulf of Mexico to sea-level rise and climate change: Implications for future change. *Mar. Geol.* **352**, 348–366 (2014).
25. J. C. Van Wagoner, Sequence stratigraphy and marine to nonmarine facies architecture of foreland basin strata, Book Cliffs, Utah, U.S.A.: Reply1. *Am. Assoc. Pet. Geol. Bull.* **82**, 1607–1618 (1998).
26. T. Muto, R. J. Steel, Autogenic response of fluvial deltas to steady sea-level fall: Implications from flume-tank experiments. *Geology* **32**, 401–404 (2004).
27. A. G. Nijhuis *et al*., Fluvio-deltaic avulsions during relative sea-level fall. *Geology* **43**, 719–722 (2015).
28. D. Mohrig, P. L. Heller, C. Paola, W. J. Lyons, Interpreting avulsion process from ancient alluvial sequences: Guadalope-Matarranya system (northern Spain) and Wasatch Formation (western Colorado). *Geol. Soc. Am. Bull.* **112**, 1787–1803 (2000).
29. D. J. Jerolmack, D. Mohrig, Conditions for branching in depositional rivers. *Geology* **35**, 463–466 (2007).
30. V. Ganti, M. P. Lamb, A. J. Chadwick, Autogenic erosional surfaces in fluvio-deltaic stratigraphy from floods, avulsions, and backwater hydrodynamics. *J. Sediment. Res.* **89**, 815–832 (2019).
31. V. Ganti, Z. Chu, M. P. Lamb, J. A. Nittrouer, G. Parker, Testing morphodynamic controls on the location and frequency of river avulsions on fans versus deltas: Huanghe (Yellow River), China. *Geophys. Res. Lett.* **41**, 7882–7890 (2014).
32. J. M. Coleman, H. H. Roberts, G. W. Stone, Mississippi River delta: An overview. *J. Coast. Res.* **14**, 698–716 (1998).
33. T. Muto, R. J. Steel, Principles of regression and transgression: The nature of the interplay between accommodation and sediment supply. *J. Sediment. Res.* **67**, 994–1000 (1997).
34. T. Muto, R. J. Steel, Role of autoretreat and A/S changes in the understanding of deltaic shoreline trajectory: A semi-quantitative approach. *Basin Res.* **14**, 303–318 (2002).
35. G. Parker, T. Muto, Y. Akamatsu, W. E. Dietrich, J. W. Lauer, Unravelling the conundrum of river response to rising sea-level from laboratory to field. Part I: Laboratory experiments. *Sedimentology* **55**, 1643–1655 (2008).
36. G. Parker, T. Muto, Y. Akamatsu, W. E. Dietrich, J. W. Lauer, Unravelling the conundrum of river response to rising sea-level from laboratory to field. Part II. The Fly–Strickland River system, Papua New Guinea. *Sedimentology* **55**, 1657–1686 (2008).
37. W. Kim, C. Paola, V. R. Voller, J. B. Swenson, Experimental measurement of the relative importance of controls on shoreline migration. *J. Sediment. Res.* **76**, 270–283 (2006).
38. J. B. Swenson, C. Paola, L. Pratson, V. R. Voller, B. A. Murray, Fluvial and marine controls on combined subaerial and subaqueous delta progradation: Morphodynamic modeling of compound-clinoform development. *J. Geophys. Res. Earth Surf.* **110**, F02013 (2005).
39. T. Muto, Shoreline autoretreat substantiated in flume experiments. *J. Sediment. Res.* **71**, 246–254 (2001).
40. D. J. Jerolmack, J. B. Swenson, Scaling relationships and evolution of distributary networks on wave-influenced deltas. *Geophys. Res. Lett.* **34**, L23402 (2007).
41. V. Ganti, A. J. Chadwick, H. J. Hassenruck-Gudipati, B. M. Fuller, M. P. Lamb, Experimental river delta size set by multiple floods and backwater hydrodynamics. *Sci. Adv.* **2**, e1501768 (2016).
42. V. Ganti, A. J. Chadwick, H. J. Hassenruck-Gudipati, M. P. Lamb, Avulsion cycles and their stratigraphic signature on an experimental backwater-controlled delta. *J. Geophys. Res. Earth Surf.* **121**, 1651–1675 (2016).
43. M. D. Reitz, D. J. Jerolmack, J. B. Swenson, Flooding and flow path selection on alluvial fans and deltas. *Geophys. Res. Lett.* **37**, L06401 (2010).
44. M. D. Reitz *et al*., Effects of tectonic deformation and sea level on river path selection: Theory and application to the Ganges-Brahmaputra-Meghna River Delta. *J. Geophys. Res. Earth Surf.*, 10.1002/2014JF003202 (2015).
45. G. Salter, C. Paola, V. R. Voller, Control of delta avulsion by downstream sediment sinks. *J. Geophys. Res. Earth Surf.* **123**, 142–166 (2018).
46. D. A. Edmonds, R. L. Slingerland, Mechanics of river mouth bar formation: Implications for the morphodynamics of delta distributary networks. *J. Geophys. Res. Earth Surf.* **112**, 1–14 (2007).
47. A. Tejedor, A. Longjas, I. Zaliapin, E. Foufoula-Georgiou, Delta channel networks: 2. Metrics of topologic and dynamic complexity for delta comparison, physical inference, and vulnerability assessment. *Water Resour. Res.* **51**, 4019–4045 (2015).
48. M. D. Reitz, D. J. Jerolmack, Experimental alluvial fan evolution: Channel dynamics, slope controls, and shoreline growth. *J. Geophys. Res.* **117**, F02021 (2012).
49. D. A. Edmonds, R. L. Slingerland, J. Best, D. Parsons, N. Smith, Response of river-dominated delta channel networks to permanent changes in river discharge. *Geophys. Res. Lett.* **37**, L12404 (2010).
50. R. L. Caldwell, D. A. Edmonds, The effects of sediment properties on deltaic processes and morphologies: A numerical modeling study. *J. Geophys. Res. Earth Surf.* **119**, 961–982 (2014).
51. W. Gao *et al*., Long-term cumulative effects of intra-annual variability of unsteady river discharge on the progradation of delta lobes: A modeling perspective. *J. Geophys. Res. Earth Surf.* **124**, 960–973 (2019).
52. M. Liang, C. Van Dyk, P. Passalacqua, Quantifying the patterns and dynamics of river deltas under conditions of steady forcing and relative sea level rise. *J. Geophys. Res. Earth Surf.* **121**, 465–496 (2016).
53. M. Liang, W. Kim, P. Passalacqua, How much subsidence is enough to change the morphology of river deltas? *Geophys. Res. Lett.* **43**, 10–266 (2016).
54. K. M. Ratliff, E. H. W. Hutton, A. B. Murray, Exploring wave and sea-level rise effects on delta morphodynamics with a coupled river-ocean model. *J. Geophys. Res. Earth Surf.* **123**, 2887–2900 (2018).
55. A. J. Chadwick, M. P. Lamb, A. J. Moodie, G. Parker, J. A. Nittrouer, Origin of a preferential avulsion node on lowland river deltas. *Geophys. Res. Lett.* **46**, 4267–4277 (2019).
56. A. J. Moodie *et al*., Modeling deltaic lobe-building cycles and channel avulsions for the Yellow River Delta, China. *J. Geophys. Res. Earth Surf.*, 10.1029/2019JF005220 (2019).
57. F. Engelund, E. Hansen, *A Monograph on Sediment Transport in Alluvial Streams*, (Technical University of Denmark, Copenhagen, 1967).
58. J. B. Swenson, V. R. Voller, C. Paola, G. Parker, J. G. Marr, Fluvio-deltaic sedimentation: A generalized Stefan problem. *Eur. J. Appl. Math.* **11**, 433–452 (2000).
59. S. Jelgersma, "Land subsidence in coastal lowlands" in *Sea-Level Rise and Coastal Subsidence*, (Springer, 1996), pp. 47–62.
60. J. D. Milliman, J. M. Broadus, F. Gable, Environmental and economic implications of rising sea level and subsiding deltas: The Nile and Bengal examples. *Ambio*, 340–345 (1989).
61. T. E. Törnqvist *et al*., Mississippi Delta subsidence primarily caused by compaction of Holocene strata. *Nat. Geosci.* **1**, 173–176 (2008).
62. S.-Y. Yu, T. E. Törnqvist, P. Hu, Quantifying Holocene lithospheric subsidence rates underneath the Mississippi Delta. *Earth Planet. Sci. Lett.* **331**, 21–30 (2012).
63. R. Bintanja, R. S. W. van de Wal, J. Oerlemans, Modelled atmospheric temperatures and global sea levels over the past million years. *Nature* **437**, 125–128 (2005).
64. J. P. M. Syvitski *et al*., Sinking deltas due to human activites. *Nat. Geosci.* **2**, 681–686 (2009).
65. J. D. Milliman, J. P. M. Syvitski, Geomorphic/tectonic control of sediment discharge to the ocean: The importance of small mountainous rivers. *J. Geol.* **100**, 525–544 (1992).
66. T. Muto, J. B. Swenson, Large-scale fluvial grade as a nonequilibrium state in linked depositional systems: Theory and experiment. *J. Geophys. Res. Earth Surf.* **110**, F03002 (2005).
67. C. Paola, Quantitative models of sedimentary basin filling. *Sedimentology* **47**, 121–178 (2000).
68. T. Muto *et al*., Planform evolution of deltas with graded alluvial topsets: Insights from three-dimensional tank experiments, geometric considerations and field applications. *Sedimentology* **63**, 2158–2189 (2016).
69. J. F. Bijkerk *et al*., Fluvio-marine sediment partitioning as a function of basin water depth. *J. Sediment. Res.* **86**, 217–235 (2016).
70. T. Muto, R. J. Steel, In defense of shelf-edge delta development during falling and lowstand of Relative Sea Level. *J. Geol.* **110**, 421–436 (2002).
71. E. J. Trower, V. Ganti, W. W. Fischer, M. P. Lamb, Erosional surfaces in the Upper Cretaceous Castlegate Sandstone (Utah, USA): Sequence boundaries or autogenic scour from backwater hydrodynamics? *Geology* **46**, 707–710 (2018).
72. J. Mossa, Historical changes of a major juncture: Lower Old River, Louisiana. *Phys. Geogr.* **34**, 315–334 (2013).
73. P. R. Shukla *et al*., Eds., Climate change and land: An IPCC special report on climate change, desertification, land degradation, sustainable land management, food security, and greenhouse gas fluxes in terrestrial ecosystems (Intergovernmental Panel on Climate Change, 2019).